JCTC Journal of Chemical Theory and Computation

ARTICLE

pubs.acs.org/JCTC

Adaptive-Partitioning Redistributed Charge and Dipole Schemes for QM/MM Dynamics Simulations: On-the-fly Relocation of Boundaries that Pass through Covalent Bonds

Soroosh Pezeshki and Hai Lin*

Chemistry Department, University of Colorado Denver, Denver, Colorado 80217-3364, United States

Supporting Information

ABSTRACT: Recently, Heyden, Lin, and Truhlar (*J. Phys. Chem. B* **2007**, *111*, 2231−2241) formularized the adaptive-partitioning schemes for quantum mechanical and molecular mechanical (QM/MM) molecular dynamics simulations. The adaptive-partitioning schemes permit on-the-fly reclassification of atoms/groups as part of the QM or MM subsystems during dynamics simulations. Test simulations of argon atoms in a periodic box with dual-level MM potentials in the microcanonical ensemble demonstrated that the adaptive-partitioning schemes conserved energy and momentum, which is critical to ensure correct sampling of configuration spaces of desired ensembles. In this work, we reported the extension of the adaptive-partitioning schemes to deal with groups that are molecular fragments. The newly developed adaptive-partitioning redistributed charge scheme and adaptive-partitioning redistributed charge and dipole schemes allow on-the-fly relocation of the QM/MM boundaries that cut through covalent bonds during dynamics simulations. Test QM/MM simulations with a variety of QM levels of theory in the microcanonical ensembles demonstrated that the new schemes conserve energy and momentum.

1. INTRODUCTION

The past decade has witnessed rapid growth in the applications of combined quantum mechanical and molecular mechanical (QM/MM)[1−15] methods. But conventional QM/MM methods have noticeable limits.[16] One of those limits is the prohibition of on-the-fly reclassification of atoms/groups as part of the QM or MM subsystems during molecular dynamics (MD) simulations. For many systems with localized active sites, such a limit is not a concern, but for other systems with nonlocalized active sites, such as ion solvation and transport, defect propagation in materials, and diffusion on catalytic surfaces, such a limit would require the use of large-size QM subsystems, which is very expensive or impractical at all.

Recently, there have been increasing interests in the development of new QM/MM schemes that go beyond this limit.[17−22] Several algorithms have been published on the dynamically partitioning of atoms/groups into QM or MM subsystems in MD simulations.[17−20] When an atom changes its QM or MM identity, the potential energy and forces will show sudden changes. Note that not just the force on the given atom is changing but also the forces on all the other atoms are changing. The discontinuities in energy and forces could lead to numerical instability in MD simulations.[19] Moreover, it could prevent correct sampling of configuration space of the desired ensemble.[19] To cope with those discontinuities, a narrow buffer zone (also called switching shell) is identified between the QM subsystem (also called active zone) and the MM subsystems (also called environmental zone). As illustrated in Figure 1, the active zone is usually defined as a sphere of the inner radius R_{min} centered at a given primary atom (or a given spatial location defined by the cartersian coordinates), and the buffer zone is defined as a shell within the inner and outer radii R_{min} and R_{max}. Various smoothing algorithms are applied to remove the discontinuities in the potential energy and/or forces when atoms/groups enter or leave the buffer zone. The smoothing functions, which take forms ranging from simple polynomials to complicated functions, usually depend on the distances (R_i) between the active-zone center and the atoms/groups in the buffer zone.

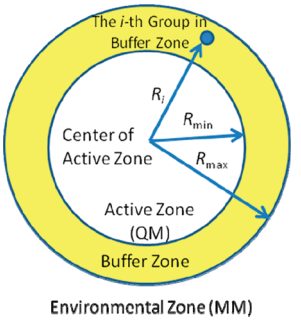

Figure 1. Illustration of the active, buffer, and environmental zones.

The "hot-spot" method[17] developed by Rode and co-workers in 1996 is one of those examples. Although this method does not conserve momentum and the energy is not evaluated or defined, for simulations in the canonical (*NVT*) ensemble, the kinetic energy is approximately constant, and the numerical instabilities are reduced. The hot-spot method has been applied in a series of studies on the ion solvation, e.g., Li^+ in ammonia,[17] Ca^{2+},[23] Na^+ and K^+,[24] Cu^{2+},[25,26] Mn^{2+},[27] Ni^{2+},[28] Li^+,[29] V^{2+},[30] Fe^{2+} and Fe^{3+},[31] F^- and Cl^-,[32,33] NO_3^-,[34] and $HCOO^-$ in water.[35] In 2002, in discussion of the hot-spot method, Kerdcharoen and Morokuma suggested the ONIOM-XS method,[18] which does

Received: July 27, 2011
Published: September 19, 2011

conserve momentum. The ONIOM-XS scheme was tested with Li^+ ion[18] and Ca^{2+} ion[36] in liquid ammonia in the isothermal−isobaric (*NPT*) ensemble. However, the ONIOM-XS scheme does not conserve energy in microcanonical (*NVE*) simulations if two or more groups are present in the buffer zone. In 2007, Heyden, Lin, and Truhlar[19] proposed two adaptive-partitioning (AP) schemes, the permuted AP and the sorted AP schemes. Those two schemes were tested by MD simulations of argon atoms in a periodic box using dual-level MM (MM/MM) potentials—the interactions between argon atoms in the active zone were described by a Morse potential and the interactions in the environmental zone by a Lennard-Jones potential. Simulations in the *NVE* ensemble demonstrated that the AP schemes conserved energy and momentum much better than the other schemes in comparison. Bulo et al.[20] introduced in 2009 the so-called difference-based adaptive solvation potential, which is related to the sorted AP scheme with a different way in constructing smoothing functions. They also put forward an interesting idea, the continuous-force scheme, which, although not energy conserving, retains a related conserved quantity (energy corrected by a book-keeping term obtained by integration of forces over the trajectory). The methods were tested by dual-level MM simulations in the *NVE* ensemble of a water-in-water model system and of an acetonitrile-in-water system.

In views of the above methods, it is clear that simulations in the *NVE* ensemble is a stricter test for the algorithms, because coupling with a heat bath in the *NVT* and *NPT* simulations will help to keep the kinetic energy approximately constant, reducing numerical instabilities. In the thermodynamics limit, calculations in different ensembles should converge; we have observed in ref 19 that the methods conserving energy and momentum produced very similar radial distribution functions in the *NVE* and *NVT* simulations of the Ar system, while methods with poor conservation of energy and momentum did not. Schemes that do not conserve energy or momentum might still be useful in *NVT* and *NPT* simulations, if proper care is taken to avoid/minimize artifacts in the results.

All methods discussed so far only deal with groups that are whole molecules, such as water and ammonia. A question remains unanswered: What to do if one wants to define a fragment of a molecule as a group? For example, can we define the backbone or side chain of a residue in a protein to be a group? Doing so requires that one must be able to dynamically relocate the QM/MM boundary that passes through covalent bonds during MD simulations. Solving the problem of "fragmental group" for QM/MM dynamics simulations is not only very interesting but also has practical uses. For example, an enzyme active site is usually modeled at the QM level in a QM/MM setup. During MD simulations, side chains of residues may flip away, cofactors may bind, products may be released, and solvent molecules may diffuse in. It will be beneficial to dynamically vary the contents of the QM subsystem in response to those conformational changes. Another example is the simulations of an ion or a molecule transport through membrane channel proteins, where it is desirable to include the ion or molecule and its first solvation shell into the QM subsystem. With the new development here, one could construct a moving QM subsystem centered at the given ion or molecule; when the ion or molecule passes by a residue or lipid, one can add the residue or part of the lipid into the QM subsystem or delete it from the QM subsystem as needed.

In this work, we report an extension of the adaptive-partitioning schemes in ref 19 to handle the fragmental groups. To our knowledge, this is the first implementation of the schemes that allow on-the-fly relocation of the QM/MM boundaries that cut through covalent bonds in MD simulations. The development results in two new QM/MM schemes, namely the adaptive-partitioning redistributed charge (AP-RC) and the adaptive-partitioning redistributed charge and dipole (AP-RCD) schemes, which are described in Section 2. Test calculations are present in Section 3. The results are analyzed in Section 4, and discussion is given in Section 5.

2. METHODOLOGY

2.1. Adaptive-Partitioning Treatments. The algorithms of the adaptive-partitioning QM/MM have been given in detail in ref 19. Briefly, in the permuted AP scheme, the potential energy is expressed in a many-body expansion manner:

$$\begin{aligned} V = {} & V^{\mathrm{A}} + \sum_{i=1}^{N} P_i (V_i^{\mathrm{A}} - V^{\mathrm{A}}) \\ & + \sum_{i=1}^{N-1} \sum_{j=i+1}^{N} P_i P_j (V_{i,j}^{\mathrm{A}} - [V^{\mathrm{A}} + \sum_{r=i,j}^{N} (V_r^{\mathrm{A}} - V^{\mathrm{A}})]) \\ & + \sum_{i=1}^{N-2} \sum_{j=i+1}^{N-1} \sum_{k=j+1}^{N} P_i P_j P_k (V_{i,j,k}^{\mathrm{A}} - (V^{\mathrm{A}} + \sum_{r=i,j,k}^{N} (V_r^{\mathrm{A}} - V^{\mathrm{A}}) \\ & + \sum_{(p,q)=(i,j),(i,k),(j,k)}^{N-1,N} (V_{p,q}^{\mathrm{A}} - (V^{\mathrm{A}} \\ & + \sum_{r=i,j}^{N} (V_r^{\mathrm{A}} - V^{\mathrm{A}})))) + \ldots \end{aligned} \tag{1}$$

where V^{A} is the energy determined with the groups in the active zone at the QM level, V_i^{A} with all active-zone groups and the *i*-th buffer-zone group at the QM level, $V_{i,j}^{\mathrm{A}}$ with all active-zone groups, the *i*-th buffer-zone group, and the *j*-th buffer-zone group at the QM level, ... $V_{1,2,\ldots N}^{\mathrm{A}}$ with all active-zone groups and all *N* buffer-zone groups at the QM level, and P_i is the smoothing function of the *i*-th buffer-zone group in terms of the dimensionless reduced radial coordinate α_i:

$$\begin{aligned} P_i(\alpha_i) &= -6\alpha_i^5 + 15\alpha_i^4 - 10\alpha_i^3 + 1 \\ \alpha_i &= \frac{R_i - R_{\min}}{R_{\max} - R_{\min}} \quad \text{for } R_{\min} < R_i < R_{\max} \end{aligned} \tag{2}$$

eq 1 can be conveniently rewritten as

$$\begin{aligned} V = {} & V^{\mathrm{A}}(1 - \sum_{i=1}^{N} P_i + \sum_{i=1}^{N-1} \sum_{j=i+1}^{N} P_i P_j \\ & - \sum_{i=1}^{N-2} \sum_{j=i+1}^{N-1} \sum_{k=j+1}^{N} P_i P_j P_k + \ldots) \\ & + \sum_{i=1}^{N} P_i V_i^{\mathrm{A}} (1 - \sum_{j\neq i}^{N} P_j + \sum_{j\neq i}^{N-1} \sum_{k=j+1\neq i}^{N} P_j P_k - \ldots) \\ & + \sum_{i=1}^{N-1} \sum_{j=i+1}^{N} P_i P_j V_{i,j}^{\mathrm{A}} (1 - \sum_{k\neq i\neq j}^{N} P_k + \ldots) + \ldots \end{aligned} \tag{3}$$

or

$$V = V^{A}\prod_{i=1}^{N}(1-P_i) + \sum_{i=1}^{N} P_i V_i^{A}\prod_{j\neq i}^{N}(1-P_j) + \sum_{i=1}^{N-1}\sum_{j=i+1}^{N} P_i P_j V_{i,j}^{A}\prod_{k\neq j\neq i}^{N}(1-P_k) + \quad ... \tag{4}$$

Note the constraint that the sum of the smoothing functions is always 1.

$$\prod_{i=1}^{N}(1-P_i) + \sum_{i=1}^{N} P_i\prod_{j\neq i}^{N}(1-P_j) + \sum_{i=1}^{N-1}\sum_{j=i+1}^{N} P_i P_j\prod_{k\neq j\neq i}^{N}(1-P_k) + \quad ... = \prod_{i=1}^{N}((1-P_i) + P_i) = 1 \tag{5}$$

In total, 2^N QM calculations are to be performed. All derivatives of the potential energy with respect to the coordinates vary smoothly up to the same order for which the smoothing functions P_i vary continuously. Since $0 < P_i < 1$, the energy contributions of the terms in the series in eq 1 decrease rapidly, it may be advisible to truncate the series. The truncation significantly reduces the number of embedded QM calculations, but it also introduces small (but controllable) discontinuities in the energy and the derivatives. Our test calculations showed that the discontinuities are insignificant if the series is truncated at the fifth order. That is, only up to five groups in the buffer zone are included in the QM calculations, and the fifth or higher order terms of P_i are neglected.

In the sorted-AP scheme,[19] the groups in the buffer zone are sorted in a canonical order with respect to R_i from the smallest to largest. The QM calculations begin with the active zone only, and the buffer-zone groups are added one at a time according to the increasing distance, leading to in total $N + 1$ calculations. The potential energy in sorted AP is given by

$$V = \sum_{i=0}^{N}(\Phi_i V_{1,2}^{A}{}_{,\ ...,\ N}(\prod_{j=i+1}^{N}(1-\Phi_j))) \tag{6}$$

or

$$V = V^{A}\prod_{j=1}^{N}(1-\Phi_j) + \Phi_1 V_1^{A}\prod_{j=2}^{N}(1-\Phi_j) + \Phi_2 V_{1,2}^{A}\prod_{j=3}^{N}(1-\Phi_j) + \quad ... \tag{7}$$

with the smoothing function

$$\Phi_i = (1-\chi_i)^{-3}$$
$$\chi_i = \sum_{j=1}^{i-1}\frac{1-P_j}{P_j-P_i} + \frac{1-P_i}{P_i} + \sum_{j=i+1}^{N}\left(P_j\frac{1-P_i}{P_i-P_j}\right) \tag{8}$$

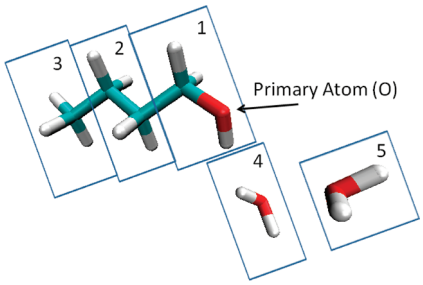

Figure 2. Groups in the test model system of a butanol in complex with two water molecules: group 1 is the $-CH_2OH$ fragment, group 2 is the $-CH_2CH_2-$ fragment, group 3 is the $-CH_3$ fragment, and groups 4 and 5 are two water molecules, respectively. The O atom in group 1 is the primary atom of the QM subsystem, i.e., the center of the active zone.

and

$$\Phi_0 \equiv 1 \tag{9}$$

The chosen smoothing function Φ_i ensures that the energy and the gradient stay constant when two groups in the buffer change the rank.

Comparing eqs 4 and 7 reveals the relationship between the permuted-AP and sorted-AP. The n-th order contributions in eq 4 comprise $W(n, N) = N!/n!(N - n)!$ number of terms, and the sorted-AP scheme keeps only one term—the term with the n buffer-zone groups that are closest to the active-zone center (presumably the biggest contribution)—with very complicated smoothing function Φ_i. Note that the sum of smoothing functions is also 1 in the sorted-AP scheme. It is also interesting to note that, if one truncates eq 3 at the first order, keeps only the constant and the linear terms of P_i, and makes the assumption that $V_1^A = V_2^A = ... = V_N^A = (1/N)V_{1,2,...,N}^A = (1/N)V^{A+B}$, then one will arrive at the energy expression for ONIOM-XS.[18]

2.2. Fragmental groups. Next, we will focus on the issues that are particularly related to the treatment of the fragmental groups. To deal with the fragmental groups in calculations, one must solve three problems. Here we illustrate the problems by using a small model system: A butanol molecule in complex with two water molecules. As shown in Figure 2, the butanol molecule is divided into three fragmental groups: $-CH_2OH$, $-CH_2CH_2-$, and $-CH_3$ as groups 1−3, while each water molecule forms a group (groups 4 and 5). The O atom in group 1 is set to be the primary atom in the QM subsystem. The distance R_i between the primary atom and the i-th group is calculated as the distance between the primary atom and the center of mass of the group (or a delegate atom of the group if needed).

The first problem is how to deal with the dangling bond at the QM/MM boundary. For example, if the boundary is passing through the C−C bond connecting groups 1 and 2 and if group 1 is the QM group, then group 1 will have a dangling bond at the boundary. Various schemes are available in the literature,[2,3,16,37−52] and here we adopt the redistributed-charge (RC) and redistributed-charge and dipole (RCD) schemes by Lin and Truhlar,[49] which are classic mechanical mimics to the quantum mechanical description of the charge distribution near the QM/MM boundary by the generalized hybrid orbital (GHO) scheme by Gao and co-workers.[40,53] In both the RC and RCD schemes, the QM subsystem is capped by a hydrogen link atom, and the MM point charge at the M1 atom (the MM atom that directly bounded to a QM atom) is evenly

redistributed to the midpoints at the M1−M2 bonds, where M2 is the MM atom that directly bond to the M1 atom. The capped group 1 becomes CH_3OH. The redistributed charges and the MM charges at the M2 atom are further modified in the RCD scheme to preserve the M1−M2 bond dipoles. Despite their simplicities, the RC and RCD schemes have been found to yield reasonably good accuracy in energies and geometries in QM/MM calculations.[49] More details about the RC and RCD schemes can be found in ref 49 and are not repeated here.

The second problem is how to define the zeros of QM and MM energies for the fragmental groups, which are to be subtracted from the raw total energy of the QM/MM calculations. The absolute energies given by the QM calculations are several orders of magnitude larger than the MM counterparts; properly setting the zeros of energy to be subtracted is therefore critical to the calculations of energies and forces in the simulations. The zero of QM (or MM) energy for a group that is a whole molecule is straightforward to obtain, which we set to the QM (or MM) energy of the isolated molecule at its geometry optimized at the given QM level of theory (or MM force field). For a group that is part of a molecule, the situation is more complicated, and the zero of energy depends on how this group is linked to other groups of the molecule. For the butanol molecule in Figure 2, group 1 is always in the active zone, and its zero of energy is given by the capped group 1, i.e., CH_3OH:

$$E_0(\text{group1}) = E(CH_3OH) \tag{10}$$

If group 2 is present in the active or buffer zone, it will be included in some of the calculations together with group 1. In those calculations, group 2 will merge with group 1 to form a "super group" $-CH_2CH_2CH_2OH$. Consequently, the link atom will cap the merged supergroup and will be located at the boundary now between groups 2 and 3. Therefore, there will be one capped supergroup $CH_3CH_2CH_2OH$ instead of two separately capped groups CH_3OH and CH_3CH_3 in the calculations. Accordingly, the zero of energy for group 2 is obtained as the energy difference between the capped supergroup and the capped group 1, each at its optimized geometries:

$$E_0(\text{group2}) = E(CH_3CH_2CH_2OH) - E(CH_3OH) \tag{11}$$

Similarly, the zero of energy for group 3 is obtained as the energy difference between the supergroup by merging groups 1 to 3 and the supergroup by merging groups 1 and 2:

$$E_0(\text{group3}) = E(CH_3CH_2CH_2CH_2OH) - E(CH_3CH_2CH_2OH) \tag{12}$$

Apparently, the zero of energy of a fragmental group must be obtained in accord to how the group is merged with other groups in the active and buffer zones. For example, if the C atom in group 3 is set to be the primary atom of the QM subsystem, we will have

$$E_0(\text{group1}) = E(CH_3CH_2CH_2CH_2OH) - E(CH_3CH_2CH_3) \tag{13}$$

$$E_0(\text{group2}) = E(CH_3CH_2CH_3) - E(CH_4) \tag{14}$$

$$E_0(\text{group3}) = E(CH_4) \tag{15}$$

This then gives rise to the third problem, which is a technical issue, that the computer program must be able to automatically relocate the boundary and find the correct zero of energy based on the topology of the system. This becomes quite cumbersome if a group is linked to many other groups via covalent bonds.

When determining the zero of energy for a fragmental group, it was not necessary to include groups that were present in the active and/or buffer zones but did not covalently connect to the fragmental group. Inclusion of those groups changed the zero of energy slightly but seemed to have negligible effects on the energy and momentum conservations in the MD simulations.

The total zero of energy for the whole system, $E_0(\text{sys})$, is the sum of the zeros of energy for all groups, according to eq 4 for the permuted-AP method and eq 8 for the sorted-AP method. A group in the buffer zone has dual (QM and MM) characteristics, so its contribution to the total zero of energy varies when its distance to the active-zone center changes. As a result, the total zero of energy for the whole system can change significantly (a few to a few hundreds of hartree, depending on the system) and rapidly (in a few tens of femtoseconds) during simulations, presenting a challenge in maintaining numerical precision and stabilities in long-time simulations, especially the *NVE* simulations. (Note that the gradients due to the smoothing functions depend on the difference between the QM and MM energies.) Such drastic variations in the zero of energy were not present in previous dual-level MM simulations,[19,20] since the zeros of MM energy of a group, such as a water molecule, are usually rather small. The numerical stability also relies critically on the availability of highly accurate gradients. Therefore, for QM calculation, a tight SCF convergence is desired. In particular, for density functional theory (DFT) calculations, fine grids for numerical integration are recommended.

The newly developed AP-RC and AP-RCD schemes have been implemented in a new version of the QMMM program.[54]

3. COMPUTATION

The energy and momentum conservations by the AP-RC and AP-RCD methods were tested by MD simulations on two model systems. The first model system was the butanol molecular in complex with two water molecules, as described in Figure 2, for which detailed analysis would be carried out. The second and larger model system was an extension of the first model system: a butanol molecule solvated in one 30 × 30 × 30 Å periodic water box of 813 water molecules, and the butanol molecule was divided into the same three fragmental groups as in the first model system. The MM force field was OPLS-AA[55−60] for butanol and TIP3P[61] for water. Table S1 in the Supporting Information lists the employed MM parameters. The QM levels of theory included the semiempirical method AM1,[62] the hartree-fock (HF) method,[63] the DFT model B3LYP,[64−66] and the post-HF method MP2.[67] The 6-31G(d) basis set[68−72] was employed for the HF, B3LYP, and MP2 calculations. As will be seen in the Results Section, basically all tested QM methods performed equally well in conserving energy and momentum of the systems. Due to high computational costs, simulations for the second model system were only carried out with AM1. In addition to the adaptive-partitioning QM/MM MD simulations, we also performed simulations at the pure-MM, the pure-QM (for the first model system only), and the fixed-partitioning QM/MM level. In the fixed-partitioning QM/MM simulations, group 1 (the $-CH_2OH$ group) was the QM subsystem while the other groups belonged to the MM subsystem. Table 1 summarizes the calculations that have been done in this work.

Table 1. List of Test Calculations[a]

entry	model system	ensemble	description	QM level	boundary treatment
1.0	first	*NVE*	pure-MM	n/a	n/a
1.1	first	*NVE*	pure-QM	AM1	n/a
1.2	first	*NVE*	fixed-partition QM/MM	AM1	RC
1.3	first	*NVE*	fixed-partition QM/MM	AM1	RCD
1.4	first	*NVE*	permuted-AP QM/MM	AM1	RC
1.5	first	*NVE*	permuted-AP QM/MM	AM1	RCD
1.6	first	*NVE*	permuted-AP QM/MM	HF/6-31G(d)	RC
1.7	first	*NVE*	permuted-AP QM/MM	HF/6-31G(d)	RCD
1.8	first	*NVE*	Permuted-AP QM/MM	B3LYP/6-31G(d)	RC
1.9	first	*NVE*	permuted-AP QM/MM	B3LYP/6-31G(d)	RCD
1.10	first	*NVE*	permuted-AP QM/MM	MP 2/6-31G(d)	RC
1.11	first	*NVE*	permuted-AP QM/MM	MP 2/6-31G(d)	RCD
2.0	second	*NVE*	pure-MM	n/a	n/a
2.1	second	*NVE*	fixed-partition QM/MM	AM1	RC
2.2	second	*NVE*	fixed-partition QM/MM	AM1	RCD
2.3	second	*NVE*	permuted-AP QM/MM	AM1	RC
2.4	second	*NVE*	permuted-AP QM/MM	AM1	RCD
2.5	second	*NVT*	pure-MM	n/a	n/a
2.6	second	*NVT*	fixed-partition QM/MM	AM1	RC
2.7	second	*NVT*	fixed-partition QM/MM	AM1	RCD
2.8	second	*NVT*	permuted-AP QM/MM	AM1	RC
2.9	second	*NVT*	permuted-AP QM/MM	AM1	RCD

[a] The first model system is a butanol molecule in complex with two water molecules (Figure 2), and the second model system is a butanol molecule in a $30 \times 30 \times 30$ Å periodic box of 813 water molecules. In the MD simulations, each trajectory was propagated using the velocity Verlet algorithm with 0.5 fs time steps for 10 000 steps. In the fixed-partitioning QM/MM simulations, group 1 (the $-CH_2OH$ fragment of the butanol molecule) was set to be the QM subsystem, while all other groups were set to be the MM subsystem. In the adaptive-partitioning QM/MM simulations, the active zone centered at the O atom of the butanol with a radius of 3.05 Å, the buffer zone had a thickness of 0.5 Å, the butanol was divided into three groups as shown in Figure 2, and each water molecule forms a group alone. The MM force field was OPLS-AA for butanol and TIP3P for water.

The QM/MM MD simulations were carried out by employing the new version of the QMMM program,[54] which for the QM calculations invoked the ORCA[73] program (for AM1) or the Gaussian03[74] program (for HF, B3LYP, and MP2) and for the MM calculations invoked the TINKER[75] program. Only the simulations with the permuted-AP method are presented here. The sorted-AP method was found to be less satisfactory in conserving energy in the *NVE* simulations due to numerical instabilities caused by two groups switching positions in the buffer zone,[19,20] and the results are omitted from this work. In the permuted-AP simulations, we did not observe noticeable difference in energy and momentum conservation between simulations employing the full energy expression and an expression truncated at the fifth order. Consequently, all the simulations presented here were done with the truncations at the fifth order. The trajectories were propagated by using the velocity Verlet algorithm,[76] and the time steps were set to 0.5 fs. Smaller time steps, such as 0.2 and 0.1 fs, had also been tested, and we found that they did equally well as the 0.5 fs time step in the energy and momentum conservations for the systems tested here; therefore, those results are not shown. The trajectories were recorded every 10 steps. Although we focused on the *NVE* ensemble, we also carried out the *NVT* simulations for the second model system, where the temperature was set to 300 K and was controlled by a Berendsen thermostat[77] with a coupling constant of 2 fs. The active zone was centered at the O atom of the butanol molecule with a radius of R_{min} = 3.05 Å, and the thickness of the buffer zone was 0.5 Å (R_{max} = 3.55 Å). The R_{min} = 3.05 Å was chosen such that group 2 entered and left the buffer zone frequently during MD simulations. The zeros of energies for the groups in butanol and for the water group are listed in Table S2 in the Supporting Information.

We note that the purpose of the test calculations is to verify the energy and momentum conservations by the AP-RC and AP-RCD schemes rather than to achieve good agreement with experimental results or with MD simulations at the pure-MM or pure-QM levels of theory. Such agreements are unlikely to achieve without optimizing selected parameters describing the interactions between the QM and MM subsystems;[14,78,79] examples of those parameters include the parameters for the van der Waals interactions between QM and MM atoms[80] and the partial atomic charge parameters that enter the effective QM Hamiltonians (as one-electron operators for the electrostatic interaction between the nuclei and electrons of the QM subsystem and the partial atomic charges of the MM subsystem).[16,51,52,81,82]

4. RESULTS

4.1. First Model System. First, we look at the *NVE* simulations by permuted-AP RC with AM1 as the QM level of theory, i.e., entry 1.4 in Table 1. An overview of the on-the-fly boundary relocation is provided by Figure 3. The initial geometry was such that group1 was in the active zone, groups 2 and 4 were in the buffer zone, and groups 3 and 5 in the environmental zone. After the simulation started, the distance between group 2 and

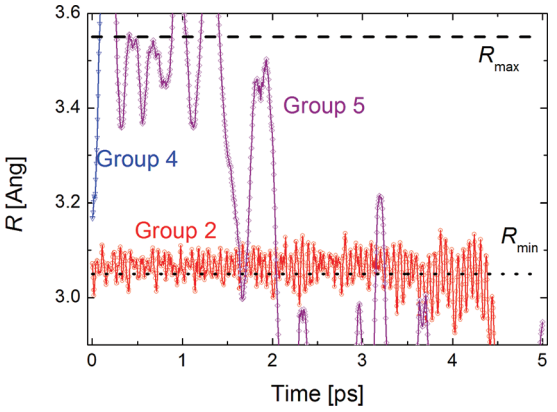

Figure 3. Respective distances between the active zone center (the O atom in butanol) and groups 2, 4, and 5 for the first model system in the *NVE* simulations by permuted-AP RC with AM1 as the QM level of theory, i.e., entry 1.4 in Table 1. The buffer zone region was between the dotted (R_{min} = 3.05 Å) and dashed (R_{max} = 3.55 Å) lines. Group 1 always stayed inside the active zone, while group 3 was outside the buffer zone during the simulation, and they are not plotted here.

the active-zone center fluctuated around 3.07 Å due to the vibrations of butanol, in particular, due to the bending of the C−C−C and O−C−C angles and the torsion of the O−C−C−C dihedral. The fast fluctuation let group 2 enter and leave the buffer zone quickly and constantly, making the model system a demanding test for the AP-RC (and AP-RCD) treatment. Soon after t = 0.075 ps, group 4 moved out of the buffer zone and stayed in the environmental zone. Group 5 then stepped into the buffer zone and after entered and left the buffer zone a few times, it eventually moved into the active zone and formed a hydrogen bond with the hydroxyl group of butanol. During the last stage of the simulation (t > 4.380 ps), group 2 walked into the active zone and resided there until the end of the simulation; visualization of the trajectory revealed that the butanol molecule underwent a noticeable conformational change from the trans to the gauche form for the bond axes of $CH_3-CH_2-CH_2-CH_2OH$. The conformational change shortened the distances between the active-zone center and groups 2 and 3 (by 0.4 and 1.2 Å, respectively).

Figure 4 shows two snapshots of the trajectory at simulation time (a) t = 0.050 ps and (b) t = 0.400 ps. In Figure 4a, group 1 ($-CH_2OH$) was in the active zone, while groups 2 ($-CH_2CH_2-$) and 4 (H_2O) were in the buffer zone. In Figure 4 b, group 2 had entered the active zone, group 4 moved into the environmental zone, and group 5 (H_2O) entered the buffer zone from the environmental zone. Group 2 then merged with group 1, producing a supergroup in the active zone: $-CH_2CH_2CH_2OH$. Clearly, the QM/MM boundary had shifted outward from at t = 0.050 to t = 0.400 ps.

The exchange of groups between the active, buffer, and environmental zones had led to significant variations in the zero of energy for the system E_0(sys). Figure 5 shows such changes in the zero of energy as a function of simulation time. Those large variations (a few thousands of kcal/mol) were caused by the water molecules due to their significant changes in R. The contributions by group 2 were smaller, usually less than 100 kcal/mol. As pointed out earlier, E_0(sys) needs to be subtracted from the raw total energy of a QM/MM calculation. Obtaining accurate E_0(sys) is therefore crucial to the success of the adaptive-partitioning QM/MM simulations.

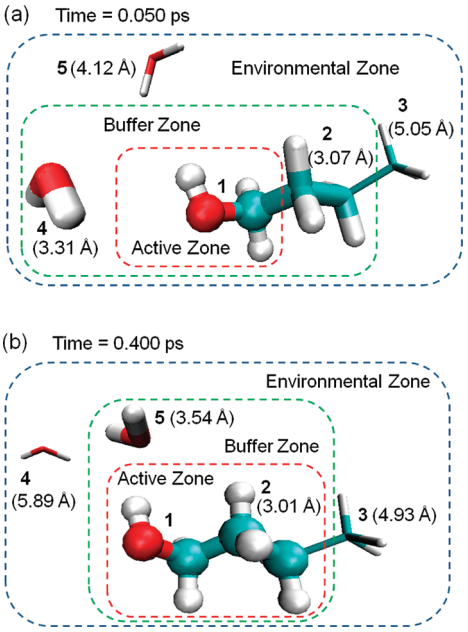

Figure 4. Snapshots at (a) t = 0.050 ps and (b) t = 0.400 ps from the *NVE* simulation by permuted-AP RC for the first model system. The QM level of theory was AM1. Groups in the active zone are shown as balls and sticks, in the buffer zone as licorice (thick), and in the environmental zone as licorice (thin). The distance between the primary atom (O in butanol) and a group (center of mass) is listed in parentheses next to the given group. The corresponding distances for group 1, which are not shown in the figure, are 0.65 Å in both (a) and (b).

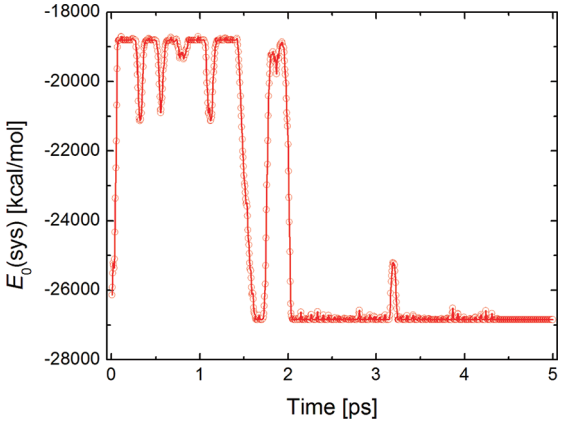

Figure 5. The zero of energy of the first model system vs simulation time for the *NVE* simulation by permuted-AP RC with AM1 as the QM level of theory, i.e., entry 1.4 in Table 1.

The conservation of energy is readily examined by plotting the total energies of the system as a function of simulation time, which was done in Figure 6 for the pure-MM (entry 1.0), pure-QM (entry 1.1), fixed-partitioning QM/MM (entries 1.2 and 1.3), and permuted-AP QM/MM (entries 1.4 and 1.5) simulations; the simulations were carried out with AM1 as the QM method. As can be seen, the performances by all methods are very similar. The fluctuations in the total energy were generally smaller than 0.1 kcal/mol. The adaptive-partitioning QM/MM schemes did not yield any notable long-term drift in the total energy during the 5 ps simulations, despite the large variations in the zeros of the energy as discussed above. As a quick and rough

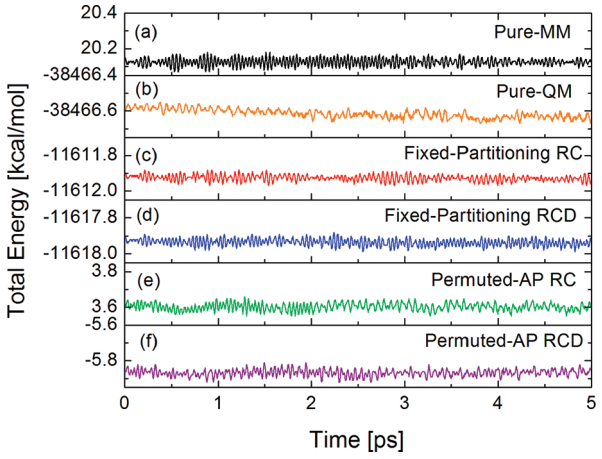

Figure 6. Total energies of the first model system in the *NVE* simulations at (a) the pure-MM, (b) the pure-QM, (c) and (d) the fixed-partitioning QM/MM, and (e) and (f) the adaptive-partitioning QM/MM levels. The QM theory was AM1. The calculations are entries 1.0−1.5 in Table 1. For the adaptive-partitioning QM/MM calculations, the zero of energy of the system E_0(sys) has been subtracted from the raw total energy.

estimation, we compared the total energies averaged over the first picosecond ($\overline{E}_{1\ \mathrm{ps}}$) and over the last picosecond ($\overline{E}_{5\ \mathrm{ps}}$). The energy difference $\Delta\overline{E} = |\overline{E}_{1\ \mathrm{ps}} - \overline{E}_{5\ \mathrm{ps}}|$ was 0.001 kcal/mol in the permuted-AP RC and 0.006 kcal/mol in the permuted-AP RCD simulations. For comparison, $\Delta\overline{E}$ was 0.001 kcal/mol for the pure-MM simulation, 0.050 kcal/mol for pure-QM, 0.009 kcal/mol for fixed-partitioning RC, and 0.010 kcal/mol for fixed-partitioning RCD, respectively. Although 5 ps is not a very long time, the above numbers do indicate that the permuted-AP RC and RCD schemes conserve energy and momentum reasonably well. Adaptive-partitioning QM/MM with higher levels of QM theory HF, B3LYP, and MP2 was tested in entries 1.6−1.11, respectively, and their total energies were displayed in Figure S1, Supporting Information. Again, very satisfactory performance has been observed. The values of $\Delta\overline{E}$ were found to be small in all six simulations: for HF, 0.007 kcal/mol in permuted-AP RC and less than 0.001 kcal/mol in permuted-AP RCD; the corresponding values were 0.007 and 0.005 kcal/mol for B3LYP and 0.004 and 0.003 kcal/mol for MP2.

4.2. Second Model System. The total energies of the *NVE* simulations for the second model system (entries 2.0−2.4) were plotted in Figure S2, Supporting Information, and the temperatures were shown in Figure S3, Supporting Information. Both the energies and temperature were found very stable, although the fluctuations were larger than those in the smaller first model system. The performances by the permuted-AP RC and permuted-AP RCD schemes seemed comparable to those by the pure-MM and by the fixed-partitioning RC and RCD schemes. We found that $\Delta\overline{E}$ was 0.1 kcal/mol for the pure-MM simulation, 0.1 kcal/mol for fixed-partitioning RC, 0.2 kcal/mol for fixed-partitioning RCD, 0.2 kcal/mol for permuted-AP RC, and 0.5 kcal/mol for permuted-AP RCD, respectively. For the *NVT* simulations (entries 2.5−2.9), the total energies and temperatures were illustrated in Figures S4 and S5, Supporting Information, respectively. The energy and momentum were reasonably well conserved, although the fluctuations in the total energy were larger than those in the *NVE* simulation. As expected, the fluctuations in the temperatures were smaller than those in the *NVE* simulations. In a similar way to $\Delta\overline{E}$, we computed for the *NVT* simulations the temperatures averaged over the first picosecond $\overline{T}_{1\ \mathrm{ps}}$ and over the last picosecond $\overline{T}_{5\ \mathrm{ps}}$, and the difference $\Delta\overline{T} = |\overline{T}_{1\ \mathrm{ps}} - \overline{T}_{5\ \mathrm{ps}}|$ was found to be 0.008, 0.005, <0.001, 0.050, and 0.040 K for entries 2.5−2.9, respectively.

5. DISCUSSION

The computational costs of the adaptive-partitioning QM/MM methods depend on the number of groups in the buffer zone.[19,20] The permuted-AP treatment is the most rigorous algorithm and provided the most satisfactory conservation of energy and momentum in our tests. Unfortunately, its computational cost scales unfavorably as 2^N, where N is number of groups in the buffer zone. One obvious way to lower the costs is to reduce the thickness of the buffer zone. For an ion solvated in water, an active zone with diameter of 9 Å and a buffer zone of 1 Å thickness will give rise to approximately 10 water molecules in the buffer zone, leading to 2^{10} = 1024 QM calculations for one time step. However, if the buffer zone can be narrowed down to 0.5 Å, there will only be 5 water molecules in the buffer zone, requiring 2^5 = 32 calculations, which is a lot less. Based on what we have found in our test calculations, the difference in the qualities of energy and momentum conservations was insignificant between a buffer of 0.5 Å thickness and one of 1.0 Å. The 0.5 Å option appeared to be a good choice. The problem of computational cost scaling seems less severe when modeling ion transport through channel proteins and when modeling conformational changes in enzyme active sites; in those examples, the numbers of buffer-zone groups are small (likely less than 5). Another way to reduce the computational cost of the permuted-AP treatments is to truncate the many-body expansion-like energy expression to a given order, as described in the Methodology Section. The results obtained in this work demonstrated that the energy and momentum were conserved reasonably well with the truncation at the fifth order. Finally, we emphasize that all the QM calculations for a given time step are parallel in nature, making large-scale parallel computation very feasible, especially on supercomputers with lots of computational nodes and CPUs. The wall time will in principle be determined by the QM calculations with the largest number of buffer groups.

The permuted-AP RC and RCD schemes belong to the electrostatic embedding QM/MM schemes,[39] where the QM subsystem is embedded in a background of atomic partial charges of the MM atoms. As a result, the QM wave function is polarized by the MM subsystem, providing a more realistic description than that by the mechanical embedding,[39] where the QM subsystem is computed in the gas phase. However, the gradient calculations for the embedded-QM subsystem are very expensive, especially when a large number of background point charges enter the effective QM Hamiltonian. Using cutoff to reduce the number of background point charges in the embedded-QM calculations should lower the computational costs. Another way to reduce the costs is to use the frozen density approximation that neglects the changes in the polarization of the density caused by the varying MM coordinates for a number of steps[83] and the density reduced to point charge approximation that uses the electrostatic potential (ESP) fitted charges[84,85] to replace the full density in the energy and gradient calculations of the electrostatic interactions between the QM and MM atoms.[83,85−89] It will be interesting to see how the gradients computed employing those approximations, although will not be as rigorous as the gradients

computed here with full density updated every step, affect the conservation of energy and momentum in MD simulations.

The current study is one of the steps toward our goal in developing the open-boundary QM/MM methods,[16] which will be a combination of the flexible-boundary treatments[16,52] and the adaptive-partitioning schemes. The flexible-boundary QM/MM methods aim to go beyond another limitation[16] in conventional QM/MM methods to permit partial charge transfer across the QM/MM boundaries. In the flexible-boundary treatments, both the QM and MM subsystems can have fractional numbers of charge, which in principle provides a more realistic picture for the charge distributions within the entire system. The marriage of the flexible-boundary treatments and the adaptive-partitioning schemes will make it possible for the QM and MM subsystem to dynamically exchange partial charges as well as atoms/groups during MD simulations. The open-boundary QM/MM would (at least in principle) facilitate the adoption of a relatively small QM subsystem in QM/MM molecular dynamics simulations, which will assist the use of high-level QM theory and/or long simulation time and could potentially lead to new insights.

■ ASSOCIATED CONTENT

Supporting Information. Table S1 lists the MM parameters used for model systems in this work, and Table S2 tabulates the zeros of energy for the groups. We plotted the total energies of the system versus simulation time for entries 1.6−1.11 in Figure S1, for entries 2.0−2.4 in Figure S2, and for entries 2.5−2.9 in Figure S4. The temperatures versus simulation time were displayed for entries 2.0−2.4 in Figure S3 and for entries 2.5−2.9 in Figure S5. This material is available free of charge via the Internet at http://pubs.acs.org.

■ AUTHOR INFORMATION

Corresponding Author

*E-mail: hai.lin@ucdenver.edu.

■ ACKNOWLEDGMENT

This work is supported by Research Corporation (CC6725) and National Science Foundation (CHE0952337). We thank Minnesota Supercomputing Institute for CPU time and access to Gaussian03. We thank Donald Truhlar and Andreas Heyden for helpful discussion.

■ REFERENCES

(1) Warshel, A.; Levitt, M. Theoretical studies of enzymic reactions: dielectric, electrostatic and steric stabilization of the carbonium ion in the reaction of lysozyme. *J. Mol. Biol.* **1976**, *103*, 227–249.

(2) Singh, U. C.; Kollmann, P. A. A combined ab initio quantum mechanical and molecular mechanical method for carrying out simulations on complex molecular systems: Applications to the $CH_3Cl + Cl^-$ exchange reaction and gas phase protonation of polyethers. *J. Comput. Chem.* **1986**, *7*, 718–730.

(3) Field, M. J.; Bash, P. A.; Karplus, M. A combined quantum mechanical and molecular mechanical potential for molecular dynamics simulations. *J. Comput. Chem.* **1990**, *11*, 700–733.

(4) Gao, J. Methods and applications of combined quantum mechanical and molecular mechanical potentials. *Rev. Comput. Chem.* **1996**, *7*, 119–185.

(5) Friesner, R. A.; Beachy, M. D. Quantum mechanical calculations on biological systems. *Curr. Opin. Struct. Biol.* **1998**, *8*, 257–262.

(6) *Combined quantum mechanical and molecular mechanical methods: ACS Symp. Ser. 712*; Gao, J., Thompson, M. A.; Eds.; American Chemical Society: Washington, DC, 1998, 310 pp.

(7) Ruiz-López, M. F.; Rivail, J. L. Combined quantum mechanics and molecular mechanics approaches to chemical and biochemical reactivity. In *Encyclopedia of computational chemistry*; von Ragué Schleyer, P., Ed.; Wiley: Chichester, U.K., 1998; Vol. 1, pp 437−448.

(8) Monard, G.; Merz, K. M., Jr. Combined quantum mechanical/molecular mechanical methodologies applied to biomolecular systems. *Acc. Chem. Res.* **1999**, *32*, 904–911.

(9) Hillier, I. H. Chemical reactivity studied by hybrid QM/MM methods. *THEOCHEM* **1999**, *463*, 45–52.

(10) Hammes-Schiffer, S. Theoretical perspectives on proton-coupled electron transfer reactions. *Acc. Chem. Res.* **2000**, *34*, 273–281.

(11) Sherwood, P. Hybrid quantum mechanics/molecular mechanics approaches. In *Modern Methods and Algorithms of Quantum Chemistry*; Grotendorst, J., Ed.; John von Neumann Institute: Jülich, 2000; Vol. 3, pp 285−305.

(12) Gao, J.; Truhlar, D. G. Quantum mechanical methods for enzyme kinetics. *Annu. Rev. Phys. Chem.* **2002**, *53*, 467–505.

(13) Morokuma, K. New challenges in quantum chemistry: quests for accurate calculations for large molecular systems. *Philos. Trans. R. Soc. London, A* **2002**, *360*, 1149–1164.

(14) Lin, H.; Truhlar, D. G. QM/MM: What have we learned, where are we, and where do we go from here? *Theor. Chem. Acc.* **2007**, *117*, 185–199.

(15) Senn, H. M.; Thiel, W. QM/MM methods for biological systems. *Top. Curr. Chem.* **2007**, *268*, 173–290.

(16) Zhang, Y.; Lin, H. Flexible-boundary QM/MM calculations: II. Partial charge transfer across the QM/MM boundary that passes through a covalent bond *Theor. Chem. Acc.* **2010**, *126*, 315–322.

(17) Kerdcharoen, T.; Liedl, K. R.; Rode, B. M. A QM/MM simulation method applied to the solution of Li^+ in liquid ammonia. *Chem. Phys.* **1996**, *211*, 313–323.

(18) Kerdcharoen, T.; Morokuma, K. ONIOM-XS: an extension of the ONIOM method for molecular simulation in condensed phase. *Chem. Phys. Lett.* **2002**, *355*, 257–262.

(19) Heyden, A.; Lin, H.; Truhlar, D. G. Adaptive partitioning in combined quantum mechanical and molecular mechanical calculations of potential energy functions for multiscale simulations. *J. Phys. Chem. B* **2007**, *111*, 2231–2241.

(20) Bulo, R. E.; Ensing, B.; Sikkema, J.; Visscher, L. Toward a practical method for adaptive QM/MM simulations. *J. Chem. Theory Comput.* **2009**, *5*, 2212–2221.

(21) Nielsen, S. O.; Bulo, R. E.; Moore, P. B.; Ensing, B. Recent progress in adaptive multiscale molecular dynamics simulations of soft matter. *Phys. Chem. Chem. Phys.* **2010**, *12*, 12401–12414.

(22) Poma, A. B.; Delle Site, L. Classical to path-integral adaptive resolution in molecular simulation: Towards a smooth quantum-classical coupling. *Phys. Rev. Lett.* **2010**, *104*, 250201.

(23) Tongraar, A.; Liedl, K. R.; Rode, B. M. Solvation of Ca^{2+} in water studied by Born-Oppenheimer ab Initio QM/MM dynamics. *J. Phys. Chem. A* **1997**, *101*, 6299–6309.

(24) Tongraar, A.; Liedl, K. R.; Rode, B. M. Born-Oppenheimer ab initio QM/MM dynamics simulations of Na^+ and K^+ in water: From structure making to structure breaking effects. *J. Phys. Chem. A* **1998**, *102*, 10340–10347.

(25) Marini, G. W.; Liedl, K. R.; Rode, B. M. Investigation of Cu^{2+} hydration and the Jahn-Teller effect in solution by QM/MM monte carlo simulations. *J. Phys. Chem. A* **1999**, *103*, 11387–11393.

(26) Schwenk, C. F.; Rode, B. M. New insights into the Jahn-Teller effect through ab initio quantum-mechanical/molecular-mechanical molecular dynamics simulations of Cu-II in water. *ChemPhysChem* **2003**, *4*, 931–943.

(27) Yagüe, J. I.; Mohammed, A. M.; Loeffler, H.; Rode, B. M. Classical and mixed quantum mechanical/molecular mechanical simulation of hydrated manganous ion. *J. Phys. Chem. A* **2001**, *105*, 7646–7650.

(28) Inada, Y.; Loeffler, H. H.; Rode, B. M. Librational, vibrational, and exchange motions of water molecules in aqueous Ni(II) solution: classical and QM/MM molecular dynamics simulations. *Chem. Phys. Lett.* **2002**, *358*, 449–458.

(29) Loeffler, H. H.; Rode, B. M. The hydration structure of the lithium ion. *J. Chem. Phys.* **2002**, *117*, 110–117.

(30) Loeffler, H. H.; Yague, J. I.; Rode, B. M. QM/MM-MD simulation of hydrated vanadium(II) ion. *Chem. Phys. Lett.* **2002**, *363*, 367–371.

(31) Remsungnen, T.; Rode, B. M. Dynamical properties of the water molecules in the hydration shells of Fe(II) and Fe(III) ions: ab initio QM/MM molecular dynamics simulations. *Chem. Phys. Lett.* **2003**, *367*, 586–592.

(32) Tongraar, A.; Rode, B. M. The hydration structures of F^- and Cl^- investigated by ab initio QM/MM molecular dynamics simulations. *Phys. Chem. Chem. Phys.* **2003**, *5*, 357–362.

(33) Tongraar, A.; Rode, B. M. Ab initio QM/MM dynamics of anion-water hydrogen bonds in aqueous solution. *Chem. Phys. Lett.* **2005**, *403*, 314–319.

(34) Tongraar, A.; Tangkawanwanit, P.; Rode, B. M. A combined QM/MM molecular dynamics simulations study of nitrate anion (NO_3^-) in aqueous solution. *J. Phys. Chem. A* **2006**, *110*, 12918–12926.

(35) Payaka, A.; Tongraar, A.; Rode, B. M. Combined QM/MM MD study of $HCOO^-$-water hydrogen bonds in aqueous solution. *J. Phys. Chem. A* **2009**, *113*, 3291–3298.

(36) Kerdcharoen, T.; Morokuma, K. Combined quantum mechanics and molecular mechanics simulation of Ca^{2+}/ammonia solution based on the ONIOM-XS method: Octahedral coordination and implication to biology. *J. Chem. Phys.* **2003**, *118*, 8856–8862.

(37) Maseras, F.; Morokuma, K. IMOMM: a new integrated ab initio + molecular mechanics geometry optimization scheme of equilibrium structures and transition states. *J. Comput. Chem.* **1995**, *16*, 1170–1179.

(38) Assfeld, X.; Rivail, J.-L. Quantum chemical computations on parts of large molecules: the ab initio local self consistent field method. *Chem. Phys. Lett.* **1996**, *263*, 100–106.

(39) Bakowies, D.; Thiel, W. Hybrid models for combined quantum mechanical and molecular mechanical approaches. *J. Phys. Chem.* **1996**, *100*, 10580–10594.

(40) Gao, J.; Amara, P.; Alhambra, C.; Field, M. J. A generalized hybrid orbital (GHO) method for the treatment of boundary atoms in combined QM/MM calculations. *J. Phys. Chem. A* **1998**, *102*, 4714–4721.

(41) Antes, I.; Thiel, W. Adjusted connection atoms for combined quantum mechanical and molecular mechanical methods. *J. Phys. Chem. A* **1999**, *103*, 9290–9295.

(42) de Vries, A. H.; Sherwood, P.; Collins, S. J.; Rigby, A. M.; Rigutto, M.; Kramer, G. J. Zeolite structure and reactivity by combined quantum-chemical-classical calculations. *J. Phys. Chem. B* **1999**, *103*, 6133–6141.

(43) Zhang, Y.; Lee, T.-S.; Yang, W. A pseudobond approach to combining quantum mechanical and molecular mechanical methods. *J. Chem. Phys.* **1999**, *110*, 46–54.

(44) Das, D.; Eurenius, K. P.; Billings, E. M.; Sherwood, P.; Chatfield, D. C.; Hodoscek, M.; Brooks, B. R. Optimization of quantum mechanical molecular mechanical partitioning schemes: Gaussian delocalization of molecular mechanical charges and the double link atom method. *J. Chem. Phys.* **2002**, *117*, 10534–10547.

(45) DiLabio, G. A.; Hurley, M. M.; Christiansen, P. A. Simple one-electron quantum capping potentials for use in hybrid QM/MM studies of biological molecules. *J. Chem. Phys.* **2002**, *116*, 9578–9584.

(46) Amara, P.; Field, M. J. Evaluation of an ab initio quantum mechanical/molecular mechanical hybrid-potential link-atom method. *Theor. Chem. Acc.* **2003**, *109*, 43–52.

(47) Sherwood, P.; de Vries, A. H.; Guest, M. F.; Schreckenbach, G.; Catlow, C. R. A.; French, S. A.; Sokol, A. A.; Bromley, S. T.; Thiel, W.; Turner, A. J.; Billeter, S.; Terstegen, F.; Thiel, S.; Kendrick, J.; Rogers, S. C.; Casci, J.; Watson, M.; King, F.; Karlsen, E.; Sjovoll, M.; Fahmi, A.; Schafer, A.; Lennartz, C. QUASI: A general purpose implementation of the QM/MM approach and its application to problems in catalysis. *THEOCHEM* **2003**, *632*, 1–28.

(48) Pu, J.; Gao, J.; Truhlar, D. G. Generalized hybrid orbital (GHO) method for combining ab Initio hartree-fock wave functions with molecular mechanics. *J. Phys. Chem. A* **2004**, *108*, 632–650.

(49) Lin, H.; Truhlar, D. G. Redistributed charge and dipole schemes for combined quantum mechanical and molecular mechanical calculations. *J. Phys. Chem. A* **2005**, *109*, 3991–4004.

(50) Shao, Y.; Kong, J. YinYang atom: A simple combined ab Initio quantum mechanical molecular mechanical model. *J. Phys. Chem. A* **2007**, *111*, 3661–3671.

(51) Zhang, Y.; Lin, H.; Truhlar, D. G. Self-consistent polarization of the boundary in the redistributed charge and dipole scheme for combined quantum-mechanical and molecular-mechanical calculations. *J. Chem. Theory Comput.* **2007**, *3*, 1378–1398.

(52) Zhang, Y.; Lin, H. Flexible-boundary quantum-mechanical/molecular-mechanical calculations: Partial charge transfer between the quantum-mechanical and molecular-mechanical subsystems. *J. Chem. Theory Comput.* **2008**, *4*, 414–425.

(53) Amara, P.; Field, M. J.; Alhambra, C.; Gao, J. The generalized hybrid orbital method for combined quantum mechanical/molecular mechanical calculations: formulation and tests of the analytical derivatives. *Theor. Chem. Acc.* **2000**, *104*, 336–343.

(54) Lin, H.; Zhang, Y.; Pezeshki, S.; Truhlar, D. G. *QMMM*, version 1.4.0, University of Minnesota: Minneapolis, MN, 2011.

(55) Jorgensen, W. L.; Maxwell, D. S.; Tirado-Rives, J. Development and testing of the OPLS all-atom force field on conformational energetics and properties of organic liquids. *J. Am. Chem. Soc.* **1996**, *118*, 11225–11236.

(56) Jorgensen, W. L.; McDonald, N. A. Development of an all-atom force field for heterocycles. Properties of liquid pyridine and diazenes. *THEOCHEM* **1998**, *424*, 145–155.

(57) McDonald, N. A.; Jorgensen, W. L. Development of an all-atom force field for heterocycles. Properties of liquid pyrrole, furan, diazoles, and oxazoles. *J. Phys. Chem. B* **1998**, *102*, 8049–8059.

(58) Rizzo, R. C.; Jorgensen, W. L. OPLS all-atom model for amines: Resolution of the amine hydration problem. *J. Am. Chem. Soc.* **1999**, *121*, 4827–4836.

(59) Kaminski, G. A.; Friesner, R. A.; Tirado-Rives, J.; Jorgensen, W. L. Evaluation and reparametrization of the OPLS-AA force field for proteins via comparison with accurate quantum chemical calculations on peptides. *J. Phys. Chem. B* **2001**, *105*, 6474–6487.

(60) Kahn, K.; Bruice, T. C. Parameterization of OPLS−AA force field for the conformational analysis of macrocyclic polyketides. *J. Comput. Chem.* **2002**, *23*, 977–996.

(61) Jorgensen, W. L.; Chandrasekhar, J.; Madura, J. D.; Impey, R. W.; Klein, M. L. Comparison of simple potential functions for simulating liquid water. *J. Chem. Phys.* **1983**, *79*, 926–935.

(62) Dewar, M. J. S.; Zoebisch, E. G.; Healy, E. F.; Stewart, J. J. P. AM1: A new general purpose quantum mechanical molecular model. *J. Am. Chem. Soc.* **1985**, *107*, 3902–3909.

(63) Roothaan, C. C. J. New developments in molecular orbital theory. *Rev. Mod. Phys.* **1951**, *23*, 69–89.

(64) Becke, A. D. Density-functional exchange-energy approximation with correct asymptotic behavior. *Phys. Rev. A* **1988**, *38*, 3098–3100.

(65) Becke, A. D. Density-functional thermochemistry. III. The role of exact exchange. *J. Chem. Phys.* **1993**, *98*, 5648–5652.

(66) Lee, C.; Yang, W.; Parr, R. G. Development of the Colle-Salvetti correlation-energy formula into a functional of the electron density. *Phys. Rev. B: Condens. Matter* **1988**, *37*, 785–789.

(67) Møller, C. M. S.; Plesset, M. S. Note on an approximation treatment for many-electron systems. *Phys. Rev.* **1934**, *46*, 618–622.

(68) Ditchfield, R.; Hehre, W. J.; Pople, J. A. Self-consistent molecular-orbital methods. IX. An extended Gaussian-type basis for molecular-orbital studies of organic molecules. *J. Chem. Phys.* **1971**, *54*, 724–728.

(69) Francl, M. M.; Pietro, W. J.; Hehre, W. J.; Binkley, J. S.; DeFrees, D. J.; Pople, J. A.; Gordon, M. S. Self-consistent molecular

orbital methods. XXIII. A polarization-type basis set for second-row elements. *J. Chem. Phys.* **1982**, *77*, 3654–3665.

(70) Clark, T.; Chandrasekhar, J.; Spitznagel, G. W.; Schleyer, P. v. R. Efficient diffuse function-augmented basis sets for anion calculations. III. The 3-21+G basis set for first-row elements, Li-F. *J. Comput. Chem.* **1983**, *4*, 294–301.

(71) Frisch, M. J.; Pople, J. A.; Binkley, J. S. Quadratic configuration interaction. A general technique for determining electron correlation energies. *J. Chem. Phys.* **1984**, *80*, 3265–3269.

(72) Hehre, W. J.; Ditchfield, R.; Pople, J. A. Self-consistent molecular orbital methods. XII. Further extensions of Gaussian-type basis sets for use in molecular orbital studies of organic molecules. *J. Chem. Phys.* **1972**, *56*, 2257–2261.

(73) Neese, F. *ORCA*, Version 2.8.0, University of Bonn: Bonn, 2011.

(74) Frisch, M. J.; Trucks, G. W.; Schlegel, H. B.; Scuseria, G. E.; Robb, M. A.; Cheeseman, J. R.; Montgomery, J., J. A.; Vreven, T.; Kudin, K. N.; Burant, J. C.; Millam, J. M.; Iyengar, S. S.; Tomasi, J.; Barone, V.; Mennucci, B.; Cossi, M.; Scalmani, G.; Rega, N.; Petersson, G. A.; Nakatsuji, H.; Hada, M.; Ehara, M.; Toyota, K.; Fukuda, R.; Hasegawa, J.; Ishida, M.; Nakajima, T.; Honda, Y.; Kitao, O.; Nakai, H.; Klene, M.; Li, X.; Knox, J. E.; Hratchian, H. P.; Cross, J. B.; Adamo, C.; Jaramillo, J.; Gomperts, R.; Stratmann, R. E.; Yazyev, O.; Austin, A. J.; Cammi, R.; Pomelli, C.; Ochterski, J. W.; Ayala, P. Y.; Morokuma, K.; Voth, G. A.; Salvador, P.; Dannenberg, J. J.; Zakrzewski, V. G.; Dapprich, S.; Daniels, A. D.; Strain, M. C.; Farkas, O.; Malick, D. K.; Rabuck, A. D.; Raghavachari, K.; Foresman, J. B.; Ortiz, J. V.; Cui, Q.; Baboul, A. G.; Clifford, S.; Cioslowski, J.; Stefanov, B. B.; Liu, G.; Liashenko, A.; Piskorz, P.; Komaromi, I.; Martin, R. L.; Fox, D. J.; Keith, T.; Al-Laham, M. A.; Peng, C. Y.; Nanayakkara, A.; Challacombe, M.; Gill, P. M. W.; Johnson, B.; Chen, W.; Wong, M. W.; Gonzalez, C.; Pople, J. A. *Gaussian03*, version E.01, Gaussian, Inc.: Pittsburgh, PA, 2003.

(75) Ponder, J. W. *TINKER*, version 5.1, Washington University: St. Louis, MO, 2010.

(76) Swope, W. C.; Andersen, H. C.; Berens, P. H.; Wilson, K. R. A computer simulation method for the calculation of equilibrium constants for the formation of physical clusters of molecules: Application to small water clusters. *J. Chem. Phys.* **1982**, *76*, 637–649.

(77) Berendsen, H. J. C.; Postma, J. P. M.; Gunsteren, W. F. v.; DiNola, A.; Haak, J. R. Molecular dynamics with coupling to an external bath. *J. Chem. Phys.* **1984**, *81*, 3684–3690.

(78) Shaw, K. E.; Woods, C. J.; Mulholland, A. J. Compatibility of quantum chemical methods and empirical (MM) water models in quantum mechanics/molecular mechanics liquid water simulations. *J. Phys. Chem. Lett.* **2009**, *1*, 219–223.

(79) Day, P. N.; Jensen, J. H.; Gordon, M. S.; Webb, S. P.; Stevens, W. J.; Krauss, M.; Garmer, D.; Basch, H.; Cohen, D. An effective fragment method for modeling solvent effects in quantum mechanical calculations. *J. Chem. Phys.* **1996**, *105*, 1968–1986.

(80) Riccardi, D.; Li, G. H.; Cui, Q. Importance of van der Waals interactions in QM/MM simulations. *J. Phys. Chem. B* **2004**, *108*, 6467–6478.

(81) Wang, B.; Truhlar, D. G. Combined quantum mechanical and molecular mechanical methods for calculating potential energy surfaces: Tuned and balanced redistributed-charge algorithm. *J. Chem. Theory Comput. 6*, 359-369.

(82) Wang, B.; Truhlar, D. G. Geometry optimization using tuned and balanced redistributed charge schemes for combined quantum mechanical and molecular mechanical calculations. *Phys. Chem. Chem. Phys. 13*, 10556-10564.

(83) Kästner, J.; Senn, H. M.; Thiel, S.; Otte, N.; Thiel, W. QM/MM free-energy perturbation compared to thermodynamic integration and umbrella sampling: Application to an enzymatic reaction. *J. Chem. Theory Comput.* **2006**, *2*, 452–461.

(84) Singh, U. C.; Kollman, P. A. An approach to computing electrostatic charges for molecules. *J. Comput. Chem.* **1984**, *5*, 129–145.

(85) Besler, B. H.; Merz, K. M., Jr.; Kollman, P. A. Atomic charges derived from semi-empirical methods. *J. Comput. Chem.* **1990**, *11*, 431–439.

(86) Zhang, Y.; Liu, H.; Yang, W. Free energy calculation on enzyme reactions with an efficient iterative procedure to determine minimum energy paths on a combined ab initio QM/MM potential energy surface. *J. Chem. Phys.* **2000**, *112*, 3483–3492.

(87) Donini, O.; Darden, T.; Kollman, P. A. QM-FE calculations of aliphatic hydrogen abstraction in citrate synthase and in solution: Reproduction of the effect of enzyme catalysis and demonstration that an enolate rather than an enol is formed. *J. Am. Chem. Soc.* **2000**, *122*, 12270–12280.

(88) Rod, T. H.; Ryde, U. Quantum mechanical free energy barrier for an enzymatic reaction. *Phys. Rev. Lett.* **2005**, *94*, 138302.

(89) Higashi, M.; Truhlar, D. G. Electrostatically embedded multi-configuration molecular mechanics based on the combined density functional and molecular mechanical method. *J. Chem. Theory Comput.* **2008**, *4*, 790–803.